Rapid defluoridation of drinking water by calcium carbonate nanoadsorbent: characterization, adsorption studies and application to real samples' treatment

Masooma Zawar, Rabia Nazir, Almas Hamid, Eder C. Lima and Muhammad Raza Shah

ABSTRACT

Groundwater contamination of fluoride is a serious global issue leading to its excessive intake and subsequently numerous adverse health issues. This research was designed to assess the efficiency of nanoadsorbent for removal of fluoride levels from water. For this purpose, calcium carbonate nanoparticles (average particle size 14.6 nm) were prepared and later applied for effective removal of fluoride from simulated as well as real drinking water (DW) samples collected from different areas of Lahore, Pakistan. The particles were characterized by powder X-ray diffraction, Fourier transform infrared spectroscopy, scanning electron microscopy/energy-dispersive X-ray spectroscopy, and atomic force microscopy. Physico-chemical parameters were studied in batch mode which revealed high adsorption capacity (i.e. 754.36 mg g^{-1}) at room temperature and neutral pH within 10 min. The kinetic isotherms (general, pseudo-first, and pseudo-second order), diffusion studies (intra-particle diffusion and particle diffusion models), and adsorption models (Langmuir, Freundlich, Liu, and Redlich–Peterson) were also applied to evaluate the suitability of adsorption process. The applicability of nanoadsorbent to fluoride-contaminated real DW samples led to 98–100% efficacy of defluoridation.

Key words | adsorption models, high adsorption capacity, kinetic models, time-efficient, water quality assessment

Masooma Zawar
Department of Environmental Sciences,
Kinnaird College for Women,
Lahore 54000,
Pakistan

Rabia Nazir (corresponding author)
Applied Chemistry Research Centre, Pakistan Council of Scientific and Industrial Research,
Lahore 54600,
Pakistan
E-mail: *rabiapcsir@yahoo.com*

Almas Hamid
Department of Environmental Sciences,
Kinnaird College for Women,
Lahore 54000,
Pakistan

Eder C. Lima
Institute of Chemistry, Federal University of Rio Grande do Sul,
91501-970 Porto Alegre, RS,
Brazil

Muhammad Raza Shah
H. E. J. Research Institute of Chemistry, International Center for Chemical and Biological Sciences,
University of Karachi,
Karachi 75270,
Pakistan

INTRODUCTION

Fluoride (F^-), an element essential in low concentrations for healthy teeth and bone development, can lead to adverse health issues when its intake exceeds permissible (1.5 mg L^{-1}, World Health Organization (WHO); $\leq$1.5 mg L^{-1}, National Standards for Drinking Water Quality, Pakistan) or in some cases desirable limits (1.0 mg L^{-1}, WHO) (Mohapatra *et al.* 2009). Health issues associated with high fluoride levels include dental caries; dental fluorosis; skeletal, brain, and kidney damage; dietary allergies; changes in deoxyribonucleic acid (DNA) structure; and stomach problems (Reardon & Wang 2000; Wang *et al.* 2004; Fawell *et al.* 2006; Oruc 2008; Barbier *et al.* 2010; Kut *et al.* 2016). Adverse impacts of fluoride contamination have also been observed in aquatic organisms (Camargo 2003).

According to an estimate, fluoride levels have considerably increased in the groundwaters of Central Asian countries including Pakistan (Bashir *et al.* 2013) leading to reported health concerns like fluorosis, impaired mental as well as physical development, bone deformities, hip fractures and kidney problems (Azizullah *et al.* 2011). Elevated

doi: 10.2166/ws.2019.196

levels of F^- in water can be attributed to anthropogenic sources (Ullah *et al.* 2009) and slow dissolution of fluoride-containing rocks in groundwater (Diesendorf *et al.* 1998) along with effluents from different industries (Banks *et al.* 1995; Edmunds & Smedley 2013). Exposure to high fluoride levels from daily intake of fluorinated drinking water (DW) puts people at high risk of encountering health issues. Worldwide fluoride consumption has increased enormously either from intake of fluoride-supplemented water or use of natural fluoridated water. There are over 30 countries consuming fluorinated water at levels that exceed the WHO permissible limit (Tiemann 2011, 2013). Hence, the United States Environment Protection Agency (EPA) has classified fluoride as a major water contaminant across the world (EPA 2009).

Different treatment technologies are currently available for defluoridation of water, such as adsorption (Bhatnagar *et al.* 2011; Bia *et al.* 2012), reverse osmosis, ion-exchange (Mohapatra *et al.* 2009), conventional (Gogoi *et al.* 2015), and electro coagulation–flocculation (Holt *et al.* 2005; Zuo *et al.* 2008; Emamjomeh & Sivakumar 2009) but these techniques are associated with one or more disadvantages such as length of time required, high maintenance cost, and production of environmental toxic by-products etc. (Maheshwari 2006; Ayoob *et al.* 2008; Li *et al.* 2011; Goswami & Purkait 2012; Jagtap *et al.* 2012; Rafique *et al.* 2012).

Recent times have seen the upsurge of nanotechnology application in many areas. Nanotechnology has proved a reliable, cost-effective, and highly efficient technique to treat DW (Rao *et al.* 2009; Ali 2012; Pontie *et al.* 2013; Kumar & Tomar 2014). For defluoridation of DW, adsorption is considered to be an efficient option compared to other technologies owing to simplicity of steps, operation, and maintenance cost (Bhatnagar *et al.* 2011; Jagtap *et al.* 2012). Moreover, nanoadsorbents result in high removal efficacy because of improved properties (Chang *et al.* 2006; Mansoori *et al.* 2008; Rao *et al.* 2009; Devi *et al.* 2014; Kumar & Tomar 2014; Adak *et al.* 2017b). Different nanoadsorbents, simple to complex, used for treating groundwater and DW with varying adsorption capacities include iron (Fe)–titanium (Ti) bimetallic oxide/magnetite (Fe_3O_4) (Zhang *et al.* 2014), aluminum oxide (Al_2O_3) (Tangsir *et al.* 2016; Hafshejani *et al.* 2017), magnesium oxide (MgO) (Oladoja *et al.* 2015), Al(III)–Fe(III)–La(III) trimetallic oxide (Adak *et al.* 2017b), iron oxide (Zhang *et al.* 2017), Fe–Ag magnetic binary oxide (Azari *et al.* 2015) and FeMgLa trimetal nanocomposite (Chen *et al.* 2018) and others (Adak *et al.* 2017a; Sani *et al.* 2017;Yan *et al.* 2017; Chen *et al.* 2018).

The present study was designed to explore new low cost nanoadsorbents for effective and efficient defluoridation of DW in short time without requirements for stringent conditions either in synthesis or in adsorption process.

MATERIALS AND METHODS

Materials

Calcium chloride ($CaCl_2{\cdot}2H_2O$) and sodium fluoride (NaF) were obtained from Fluka while sodium carbonate (Na_2CO_3) was procured from Sigma-Aldrich. Concentrated hydrochloric acid (HCl) was obtained from the Pakistan Council of Scientific and Industrial Research, Laboratories Complex. Distilled water was used for preparation of standard and experimental solutions.

Synthesis of calcium carbonate nanoadsorbent

For the preparation of calcium carbonate ($CaCO_3$) nanoadsorbent a simple modified precipitation method was adopted (Ghadam & Idrees 2013). To 0.15 M calcium chloride (16.6 g), taken in a two-necked round-bottom flask, 0.4 M $NaCO_3$ (42.4 g) solution was added drop wise, with continuous stirring over a period of 24 h. White precipitates of $CaCO_3$ formed were filtered, washed with distilled water followed by oven drying at 105 °C for 3–4 h. The precipitates were then annealed in cube furnace at 650 °C for 4–5 h to obtain off-white powder.

Nanoadsorbent characterization

Nano-adsorbency was characterized using Fourier transform infrared spectroscopy (FT-IR), powder X-ray diffraction (XRD), scanning electron microscopy (SEM)/energy-dispersive X-ray spectroscopy (EDX) and atomic force microscopy (AFM) in order to determine phase, particle size, purity, and composition. Potassium bromide

(KBr) pellets of sample were used for FT-IR spectrum (Bruker FT-IR). SEM/EDX (S3700N, Hitachi, Japan) and AFM (AFM 5500 Agilent, USA) images were taken for morphology and particle size. Powder XRD (PANalytical) was carried out using continuous mode.

Fluoride ion solution preparation

Stock solution (1,000 mg L^{-1}) of the fluoride ion (F^-) was prepared from NaF in distilled water, and further dilutions were made according to the requirements.

Batch adsorption studies

Batch adsorption studies were carried out to determine the effectiveness of adsorbent for uptake of F^- from aqueous solution. The experimental parameters were optimized for maximum adsorption by varying contact time, temperature, initial pH, initial F^- concentration, and adsorbent dose.

General procedure adopted for adsorption involved use of 25 mL F^- solution. After adjusting pH (using either 0.1 M HCl or 0.1 M NaOH), 0.1 g of adsorbent was added and contents of flask were stirred for definite time while maintaining constant temperature. Contents were Cannula filtered and filtrate was analyzed for residual F^- concentration using ion selective electrode (930, Spectrum Scientific). All the experimental data presented are averages of two readings. The percentage adsorption (A, %) and adsorption capacity, $q_{e,exp}$ (mg g^{-1}), were calculated as follows:

$$A = \frac{C_0 - C_t}{C_0} \times 100 \tag{1}$$

$$q_{e,\,exp} = \frac{(C_0 - C_i)V}{W} \tag{2}$$

where C_0 and C_i (mg L^{-1}) are the F^- concentrations before and after treatment, V (L) is volume of F^- solution taken and W (g) is the weight of adsorbent used.

Kinetic, adsorption, and diffusion models were applied to correlate the data, in line with earlier researches carried out to determine adsorption efficacy of new adsorbents (Jain *et al.* 2010; Gusmão *et al.* 2013; Keränen *et al.* 2015).

Theoretical models

Kinetic studies

General (Equation (3)), pseudo-first (Equation (4)), and pseudo-second order (Equation (5)) kinetic models in their non-linear form are applied to contact time studies.

$$q_t = q_e - \frac{q_e}{[k_N(q_e)^{n-1} \times t \times (n-1) + 1]^{\frac{1}{1-n}}} \tag{3}$$

$$\log(q_e - q_t) = \log q_e - \frac{k_1}{2.303}t \tag{4}$$

$$\left(\frac{t}{q_t}\right) = \frac{1}{k_2 q_e^2} + \frac{1}{q_e}t \tag{5}$$

where q_e (mg g^{-1}) and q_t (mg g^{-1}) are amount of adsorbent at equilibrium and at time t (min), respectively. k_N (min^{-1} ($g\,mg^{-1}$)$^{n-1}$), k_1 (min^{-1}), and k_2 ($g\,mg^{-1}\,min^{-1}$) are rate constants for general, pseudo-first order, and pseudo-second order, respectively.

Goodness of adsorption kinetic model fit was checked by standard deviation (SD), adjusted determination factor (R^2_{adj}) and non-linear Chi-square (χ^2), i.e. Equation (6):

$$\chi^2 = \sum \frac{(q_{e,\,exp} - q_{e,\,cal})^2}{q^2_{e,cal}} \tag{6}$$

where $q_{e,exp}$ and $q_{e,cal}$ are experimental and theoretical equilibrium capacity data.

Diffusion studies

Two models – an intra-particle diffusion model employing a Weber and Morris plot, i.e. q_t versus $t^{0.5}$ (Equation (7)) and a particle diffusion model based on Chanda plots, i.e. $ln\,(1 - C_t/C_e)$ versus t (Equation (8)) (Meenakshi & Viswanathan 2007; Sundaram *et al.* 2008, 2009) – were also investigated.

$$q_t = k_{id}t^{0.5} + C_i \tag{7}$$

where k_{id} (mg $g^{-1}\,min^{-0.5}$) is rate parameter of stage i and C_i

is thickness of boundary layer.

$$ln\left(1-\frac{C_t}{C_e}\right) = -k_p t \tag{8}$$

Both models are used to assess whether the retention process is controlled by pore (Equation (7)) or particle diffusion (Equation (8)).

Adsorption isotherms

Four adsorption isotherm models – Langmuir (Equation (9)), Freundlich (Equation (10)), Liu (Equation (11)), and Redlich–Peterson (R–P) (Equation (12)) – were used to determine fraction of sorbate that is partitioned between two phases, i.e. liquid and solid (Foo & Hameed 2010; Wu *et al.* 2010; Boparai *et al.* 2011; Saucier *et al.* 2015). The models can be described by following equations:

$$q_e = \frac{q_m \times K_L \times C_e}{1 + K_L \times C_e} \tag{9}$$

$$q_e = K_F \times C_e^{1/n_F} \tag{10}$$

$$q_e = \frac{q_m \times (K_g \times C_e)^{n_L}}{1 + (K_g \times C_e)^{n_L}} \tag{11}$$

$$q_e = \frac{K_{RP} \times C_e}{1 + \alpha_{RP} \times C_e^g} \tag{12}$$

where q_e (mg g^{-1}) is amount of metal adsorbed/gram of adsorbate at equilibrium, C_e (mg L^{-1}) is equilibrium concentration in solution, and q_m (mg g^{-1}) is the maximum adsorption capacity. K_L (L mg^{-1}) and K_F (mg g^{-1} (mg $L^{-1-})^{-1/nF}$) are Langmuir and Freundlich constants for determining rate of adsorption while n_F is the Freundlich dimensionless exponent. K_g (L mg^{-1}) and n_L are Liu constant and exponent, respectively. K_{RP} (L g^{-1}) and a_{RP} (mg $L^{-1})^{-g}$ are R–P constants while g is R–P exponent ($0 < g \leq 1$).

DW sampling, analysis, and treatment

A total of 30 DW samples were collected from 30 locations in the Lahore study area. Water supply in these areas is through tube wells installed in all parts of the district and is pumped directly into the distribution systems. Composite sampling technique was applied for sample collection from water taps by taking five random tap water samples (1 L) over a period of 8 h and then combining to get a composite sample. The samples were collected, coded (Table 1), preserved in bottles, and stored at 4 °C prior to analysis. The samples were analyzed for F^- using ion electrode prior to treatment; the results of analysis are presented in Figure 1.

Treatment of contaminated DW samples

DW samples (100 mL) were taken in a conical flask and, after maintaining pH between 7 and 8 (using 0.1 N HCl or 0.1 N NaOH), synthesized $CaCO_3$ nanoadsorbent (0.1 g) was added to the flask. The contents were stirred for 10 min at room temperature (RT ~ 30 °C) followed by Cannula filtration. The treated samples (filtrates) were analyzed for F^- ion concentration using ion selective electrode (930, Spectrum Scientific).

Table 1 | Sampling locations with sample codes

Sampling location	Sample code	Sampling location	Sample code
Allama Iqbal Town	S1	Lower Mall	S16
Bhatta Pind	S2	Mozang	S17
Bhobatian Chowk	S3	Model Town	S18
Defence Housing Authority (DHA) Phase-1	S4	Mughal Pura	S19
DHA Phase-6	S5	Multan Chungi	S20
DHA Phase-7	S6	Nawab Sahab	S21
Dharampura	S7	Raiwind	S22
Fareed Kot	S8	Sabzazar	S23
Garden Town	S9	Samanabad	S24
Green Town	S10	Shadhra Road	S25
Hanjar Wal	S11	Shalimar Town	S26
Harbanspura	S12	Thokar	S27
Jail Road	S13	Town Ship	S29
Johar Town	S14	Wapda Town (Phase-1)	S29
Kot Lakh Pat	S15	Yateem Khana	S30

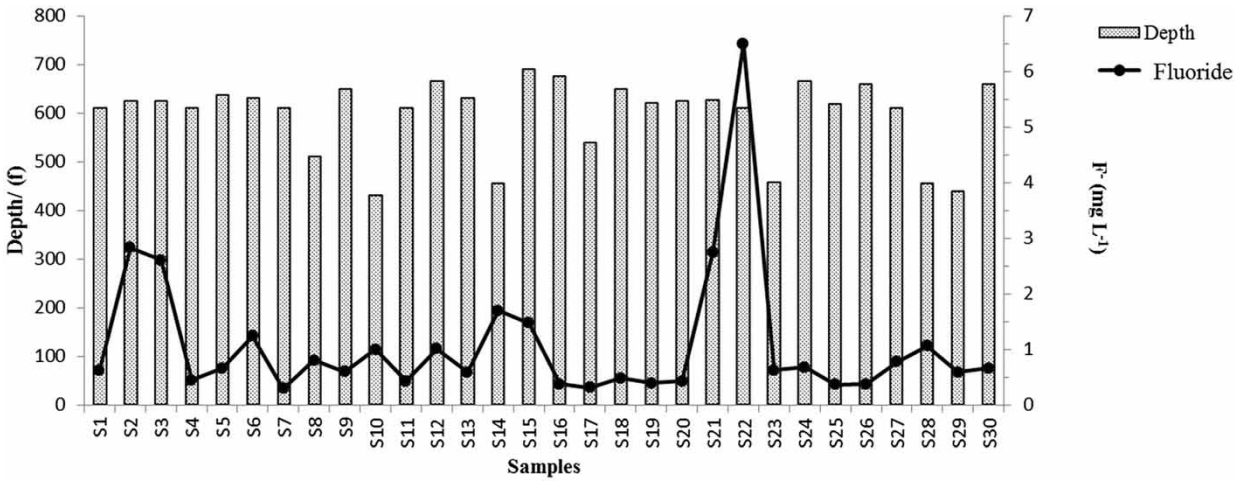

Figure 1 | DW collected from sampling area at different depths and its fluoride content and comparison with EPA's National Primary Drinking Water Regulations (EPA 2009) (–•–•–) and WHO (—) limits.

RESULTS AND DISCUSSION

Synthesis and characterization of nanoadsorbent

$CaCO_3$ nanoparticles were synthesized from $CaCl_2$ and Na_2CO_3 using simple co-precipitation procedure, which follows the ionic equation:

$$CaCl_2 + Na_2CO_3 \longrightarrow CaCO_3 \downarrow + 2NaCl$$

Prepared nanoparticles were then characterized by the following techniques:

FT-IR

The initial conformation for the synthesis of $CaCO_3$ was performed using FT-IR, the spectrum of which is presented in Figure 2(a). The spectrum shows two peaks, with the strongest peak appearing at 1,405.78 cm^{-1} and medium intensity peak at 874.69 cm^{-1}. Both peaks are attributed to bending and stretching vibrations of the O–C–O bond (Abdolmohammadi *et al.* 2012). The spectra obtained is in good agreement with the calcite characteristics peaks (Abdolmohammadi *et al.* 2012; Kirboga & Oner 2013).

Powder XRD

The powder XRD of $CaCO_3$ was performed for confirmation of phase. The diffractogram showed presence of peaks indicative of calcite (Kontoyannis & Vagenas 2000), with few peaks fitting to $Ca(OH)_2$ (Taglieri *et al.* 2013) as impurity, marked by asterisk in Figure 2(b). The diffractogram is characterized by well-defined peaks, with broadening indicating the formation of nano-sized material (Uvarov & Popov 2007).

SEM/EDX/AFM

The morphology of prepared nanoparticles, examined through SEM images (Figure 3(a)), exhibited spongy appearance of synthesized material, which might result in high adsorption capacity of F^-. Elemental composition (weight %) as determined from EDX (Figure 3(b)) was 35.83% Ca, 14.35% C, and 49.82% O, corresponding to ratio of 1:1.3:3.5 (Ca:C:O), which is in good agreement to original ratio of 1:1:3, hence confirming formation of $CaCO_3$.

The nano-size of $CaCO_3$ particles prepared was confirmed using AFM. Figure 3(c) and 3(d) presents the AFM images in both 2D and 3D view, showing particle size of 14.6 nm. The image shows narrow distribution of the particles, which have a distorted oblong shape.

Adsorption studies

Adsorption potential of nano-$CaCO_3$ was evaluated by optimizing parameters like contact time, temperature, initial pH, initial F^- concentration, and adsorbent dose.

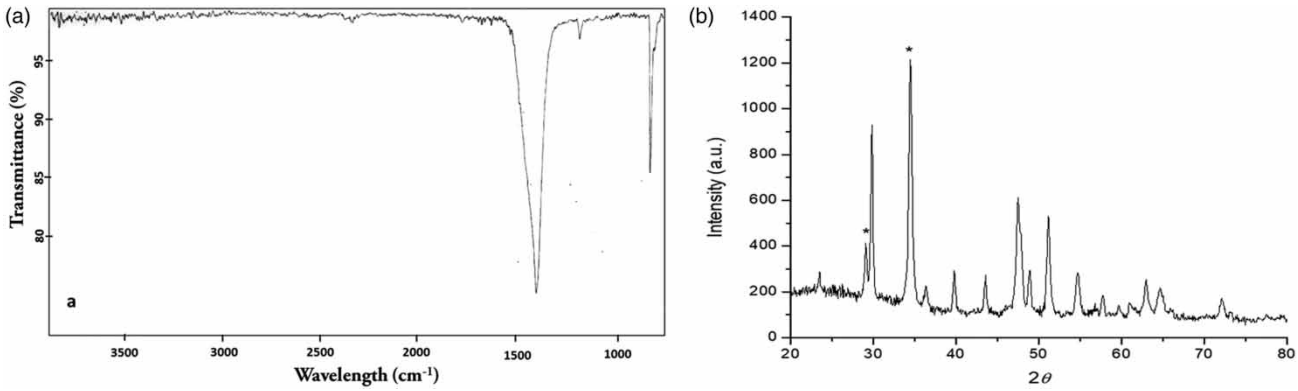

Figure 2 | $CaCO_3$ nanoparticles' (a) FT-IR spectra and (b) powder XRD matched with calcite and $Ca(OH)_2$ marked with asterisk.

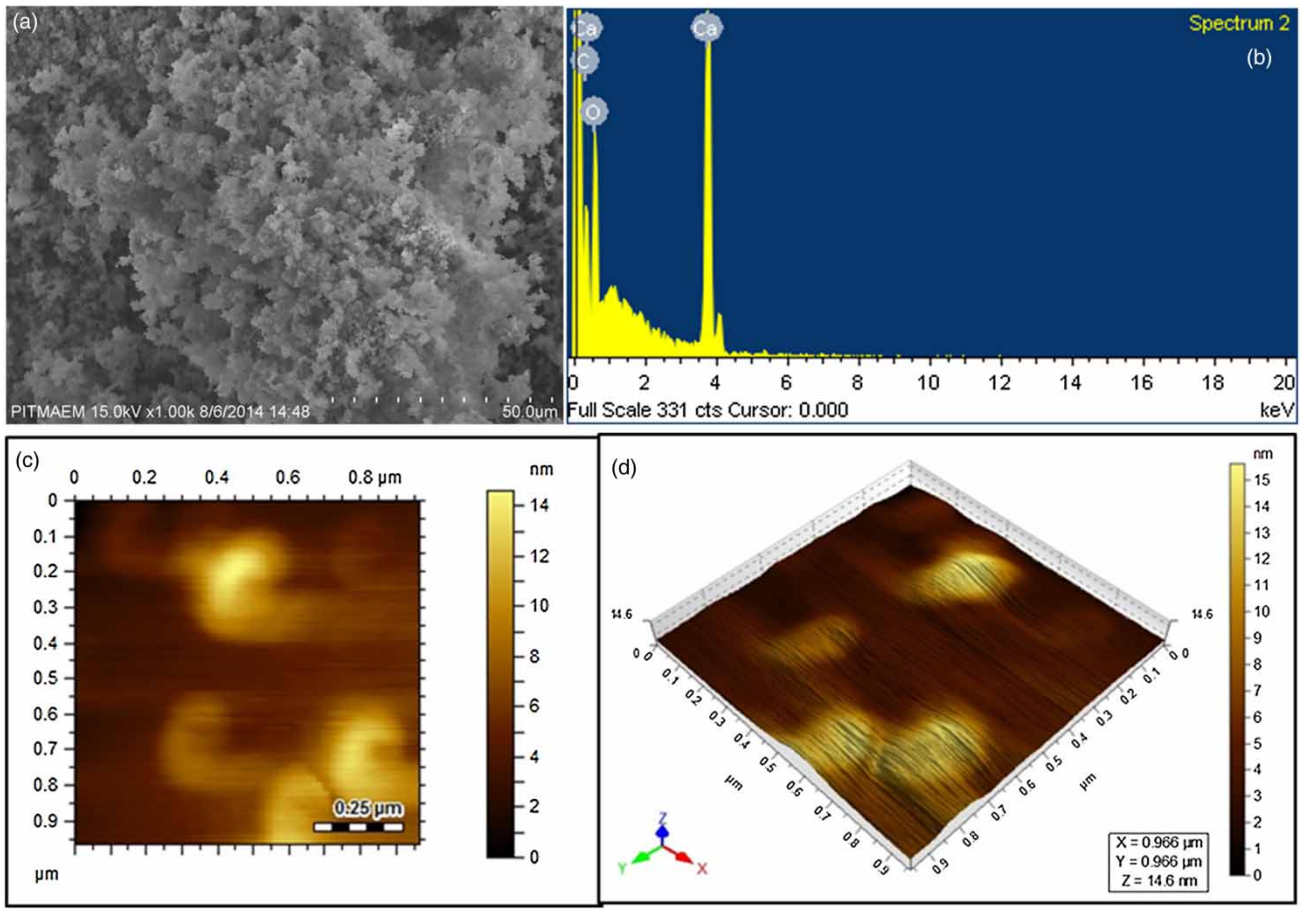

Figure 3 | (a) SEM, (b) EDX and AFM, (c) 2D and (d) 3D images of $CaCO_3$ nanoparticles showing their morphology, elemental composition, and particle size, respectively.

Effect of contact time, adsorption kinetics, and diffusion models

Room temperature batch adsorption studies were done as a function of time. The plot (Figure 4) of adsorption capacity (mg g^{-1}) against time (2–115 min) indicates rapid adsorption of F^- onto the nanoadsorbent, resulting in attainment of equilibrium within 10 min. The optimized time is much less than that already reported for other nanoadsorbents (Sundaram *et al.* 2008, 2009; Chen *et al.* 2012; Hafshejani *et al.* 2017).

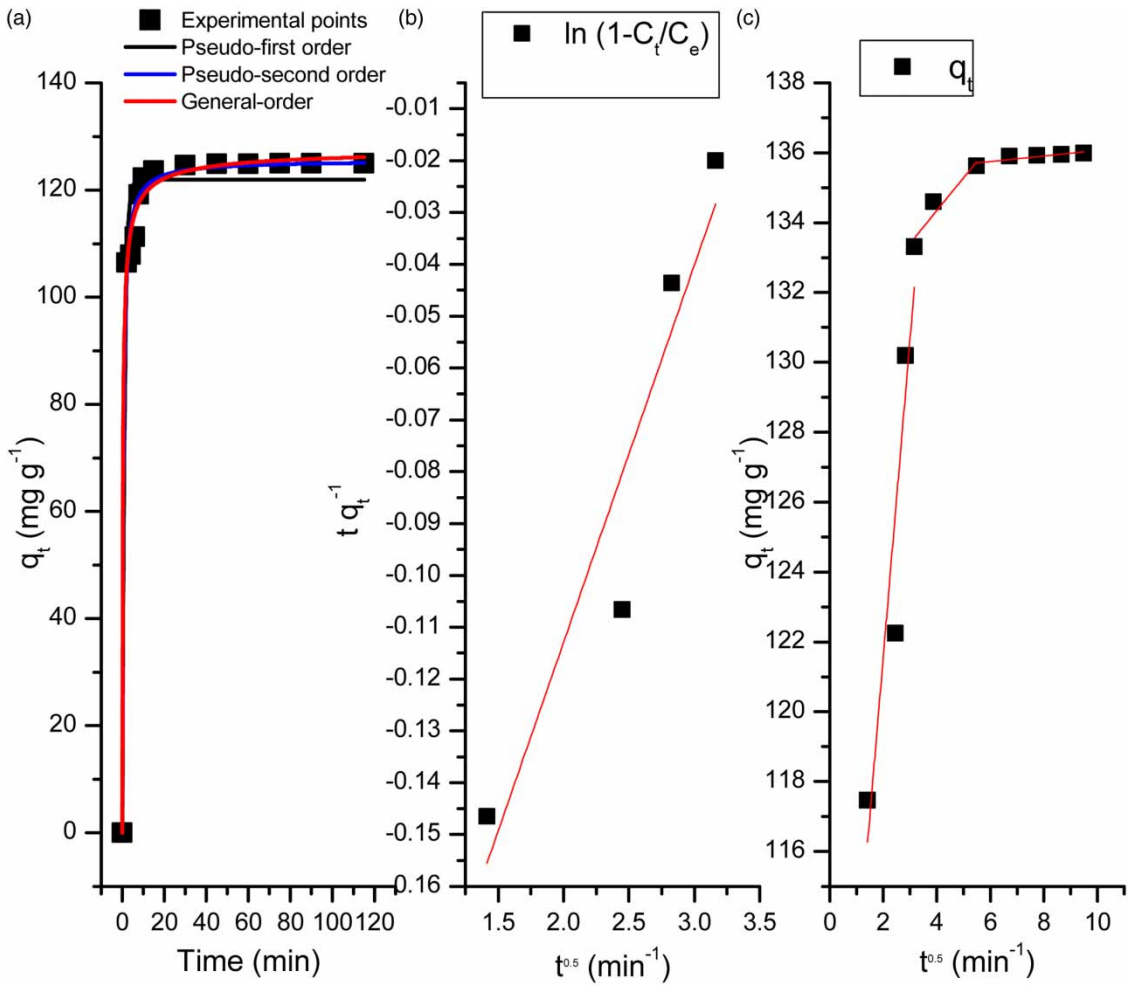

Figure 4 | Plots showing (a) effect of contact time on adsorption capacity (■) and fitting to general, pseudo first and second orders and implication of diffusion models, i.e. Chanda plots (b) and Weber and Morris plot (c).

Fitting of experimental data applied to kinetic models (general (Equation (3)), pseudo-first order (Equation (4)), and pseudo-second order (Equation (5))) and related parameters calculated in each case are given in Figure 4(a) and Table 3, respectively. The models' fitting results showed the best-fit model to be the general order compared to the rest of models based on high R^2 value, smaller standard deviation, and reduced-χ^2 value (Equation (6)) (Saucier *et al.* 2015).

The plots for particle (Equation (8)) and intra-particle (Equation (7)) diffusion models are given in Figure 4(b) and 4(c) and resulting parameters are shown in Table 2. Diffusion models give information regarding the rate-limiting step and number of processes involved in adsorption (Ciopec *et al.* 2014). The plot q_t versus $t^{0.5}$ (Figure 4(c)) showed non-linear dependency over the total range, with the line not passing through the origin, indicating the main rate-limiting step to be controlled by boundary layer diffusion. The plot is fitted to three straight lines, suggesting occurrence of different sorption phenomena (Ciopec *et al.* 2014), and depicts rapid initial adsorption owing to fast uptake of ions onto $CaCO_3$ surface, which is saturated later and leads to slower adsorption rates once equilibrium is approached. The third step corresponds to the slow process of transportation of F^{-1} into adsorbent pores (Figure 4(c)) (Ciopec *et al.* 2014). Hence the phenomenon is controlled predominantly by particle rather than pore diffusion, as also confirmed by high R^2 value (Table 3).

Table 2 | Pseudo-first and pseudo-second order parameters for fluoride adsorption on nanoadsorbent along with goodness-of-fit parameters

Model	Parameter	Value
General order	$q_{e,\exp}$ (mg g^{-1})	128.14
	k (min^{-1})	0.002
	$q_{e,\mathrm{cal}}$ (mg g^{-1})	133.30
	R^2_{adj}	0.9942
	SD	2.59
	Reduced-χ^2	6.69
Pseudo-first order	$q_{e,\exp}$ (mg g^{-1})	121.95
	k_1 (min^{-1})	0.908
	$q_{e,\mathrm{cal}}$ (mg g^{-1})	133.30
	R^2_{adj}	0.9763
	SD	5.23
	Reduced-χ^2	27.37
Pseudo-second order	$q_{e,\exp}$ (mg g^{-1})	125.54
	k_2 (min^{-1})	0.02
	$q_{e,\mathrm{cal}}$ (mg g^{-1})	133.30
	R^2_{adj}	0.9937
	SD	2.69
	Reduced-χ^2	7.26
Particle diffusion	k_p (mg g^{-1} min^{-1})	0.2117
Intra-particle diffusion	k_{id1} (mg g^{-1} min$^{-0.5}$)	9.601
	Ci_1 (mg g^{-1})	90.66
	R^2_1	0.8575
	k_{id2} (mg g^{-1} min$^{-0.5}$)	0.9406
	Ci_2 (mg g^{-1})	119.58
	R^2_2	0.8418
	k_{id3} (mg g^{-1} min$^{-0.5}$)	0.0556
	Ci_3 (mg g^{-1})	124.43
	R^2_3	0.5435

Table 3 | Langmuir, Freundlich, Liu, and R–P adsorption models constant as applied to fluoride adsorption on nanoadsorbent

Model	Parameter	Value
	$q_{e,\exp}$ (mg g^{-1})	684.76
Langmuir	K_L (L g^{-1})	281.02
	q_m (mg g^{-1})	725.21
	R^2_{adj}	0.9471
	SD (mg g^{-1})	20.06
	Reduced-χ^2	402.58
Freundlich	K_F (mg g^{-1} (mg L^{-1})$^{-1/\mathrm{nF}}$)	274.79
	n_F	4.67
	R^2_{adj}	0.9537
	SD (mg g^{-1})	54.38
	Reduced-χ^2	2,957.64
Liu	q_m (mg g^{-1})	754.36
	K_g (L mg^{-1})	0.115
	nL	0.84
	R^2_{adj}	0.9944
	SD (mg g^{-1})	17.69
	Reduced-χ^2	313.13
R–P	a_{RP} (mg L^{-1})$^{-g}$	0.16
	K (L mg^{-1})	99.80
	G	0.97
	R^2_{adj}	0.9927
	SD (mg g^{-1})	20.17
	Reduced-χ^2	6.69

Effect of temperature, initial pH and adsorbent dose

Temperature plays an important part in adsorption process considering that endothermic processes require more energy input, which makes water purification process costly. For current studies, the adsorption studies were performed by altering temperature from 30 °C to 100 °C while keeping other parameters constant ($Ci = 500$ mg L^{-1}). Figure 5(a) shows a very small incremental decrease in adsorption capacity with an increase in temperature making the adsorption phenomenon temperature-independent. Further studies were therefore performed at room temperature. This temperature-independent adsorption enhances effectiveness of the process as no extra energy is required.

To determine impact of pH on adsorption capacity of $CaCO_3$, room temperature experiments were conducted in pH range of 1–14 with 500 mg L^{-1} fluoride concentration using 0.1 g adsorbent. High F^- adsorption was observed at much broader range, i.e. full studied range (Figure 5(a)). Hence, pH maintenance is not required prior to water treatment. In contrast, earlier studies carried out using nanoadsorbents showed maximum adsorption either at low pH or in a narrow range (Li *et al.* 2001; Reyes Bahena *et al.* 2002; Tembhurkar & Dongre 2006; Sundaram *et al.* 2008; Bhatnagar *et al.* 2011).

The effect of nanoadsorbent dose was investigated by varying its amount from 0.01 to 0.125 g. Results (Figure 5(a)) indicate that with an increase in adsorbent dose the percentage of fluoride adsorption rises and reaches equilibrium at 0.025 g. An increase in amount of adsorbent is directly proportional to surface area, leading to enhancement in adsorption percentage (Tembhurkar & Dongre 2006). For further studies this optimized dose was used.

Effect of adsorbate initial concentration and adsorption isotherms

To determine the effect of initial adsorbate concentration on adsorption efficiency of nanoadsorbent, different F^-

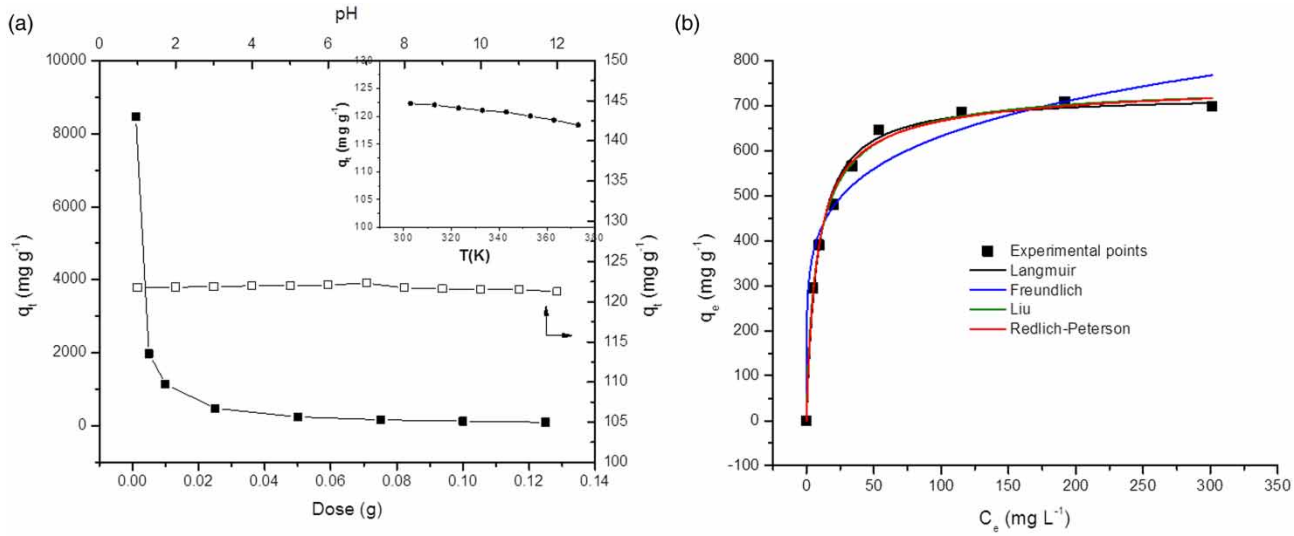

Figure 5 | (a) Effect of different parameters temperature (●), initial pH (□) and adsorbent dose (■) on adsorption capacity of $CaCO_3$; (b) Effect of adsorbate concentration on adsorption capacity, q_e, as applied to Langmuir, Freundlich, Liu and R–P adsorption models.

concentrations were treated with optimized adsorbent dose, i.e. 0.025 g, and the q_e value obtained thereafter showed optimized value at 800 mg L^{-1}. To get insight into phenomenon involved in this adsorption, various models were applied; plots and results of these studies are presented in Figure 5(b) and Table 3 respectively. The best-fit model was assessed from a high R^2 value, smaller SD, and reduced-χ^2 value.

The four adsorption models employed (Langmuir (Equation (9)), Freundlich (Equation (10)), Liu (Equation (11)), and R–P (Equation (12))) showed R^2_{adj} values in range of 0.9537–0.9927 (Figure 5(b), Table 3). The data fits well to the Liu model, with the highest R^2_{adj} and smallest reduced-χ^2 value and a q_m of 754.36 mg g^{-1} (Table 3), which is very high compared to previously reported nanoadsorbents, i.e. 2.22, 2.84, 14.9, 47.0, and 91.04 mg g^{-1} for iron–aluminum–cerium (Chen *et al.* 2009), nano-hydroxyapatite/chitin (Sundaram *et al.* 2009), Al_2O_3/CNT (Li *et al.* 2001), Fe–Ti oxide (Chen *et al.* 2012), magnetic core-shell Ce-Ti@Fe_3O_4 (Abo Markeb *et al.* 2017), respectively. The higher bonding of adsorbate with adsorbent is also denoted by high value of n_F obtained from the Freundlich isotherm (Figure 5(b), Table 3) (Khalid *et al.* 2015). The g value (close to unity) obtained in the R–P model implies monolayer adsorption behavior and compatibility with Langmuir rather than Freundlich as also indicated by the R^2_{adj} value (El-Sikaily *et al.* 2007; Amrhar *et al.* 2015).

Water samples analysis and their adsorption studies

To assess the potential of nanoadsorbent in removing F^- from real water samples, 30 water samples were collected and treated under optimized conditions (contact time 15 min, room temperature, pH 7–8). The concentration of F^- was measured before and after treatment.

According to EPA (2009) the maximum contaminant level allowed is 4 mg L^{-1}, while according to the WHO water quality guidelines, the acceptable concentration is 1.5 mg L^{-1}. Out of 30 samples, only six samples exceeded the WHO limits and one sample was above the

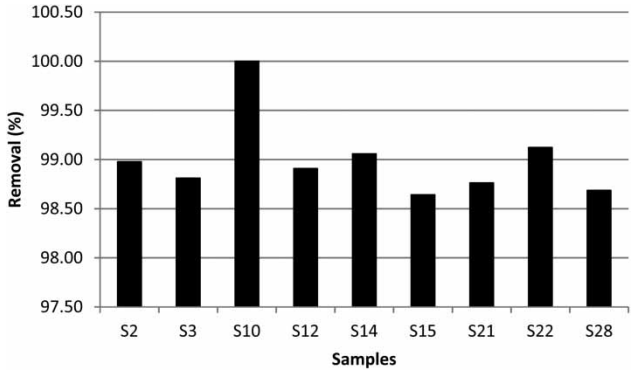

Figure 6 | Percentage removal of fluoride in real water samples after treatment with nanoadsorbent.

EPA limits. Only nine samples, with F^- concentration above 1.0 mg L^{-1}, were subjected to adsorption. The results (Figure 6) showed efficacy of nanoadsorbant by appreciable reduction in F^- level. The fluoride concentration in samples (6.497–0.999 mg L^{-1}) reduced to 0.057–0 mg L^{-1} after treatment.

CONCLUSION

$CaCO_3$ nanoparticles (14.6 nm) were prepared by a simple co-precipitation route for the defluoridation of DW. Adsorption studies at room temperature showed high adsorption capacity, i.e. 725.21 mg g^{-1}, attained in a short time. Application for treatment of actual water samples also demonstrated 98–100% removal.

FUTURE PROSPECTS

The current research dealt with exploiting the potential of prepared $CaCO_3$ nanoparticles toward F^- removal in simulated as well as real samples. The findings have opened up new dimensions for an easy and effective water defluoridation technique. In future, the studies can be extended to different dimensions to enhance its fruitfulness, as detailed below:

- Evaluating the effectiveness of prepared nanoparticles using continuous flow studies by varying the volume of water influx.
- Binding the $CaCO_3$ nanoparticles into some high surface area material for making an adsorbent bed in order to avoid the filtration challenge posed by use of nanoparticles.

REFERENCES

Abdolmohammadi, S., Siyamak, S., Ibrahim, N. A., Yunus, W. M. Z. W., Rahman, M. Z. A., Azizi, S. & Fatehi, A. 2012 Enhancement of mechanical and thermal properties of polycaprolactone/chitosan blend by calcium carbonate nanoparticles. *International Journal of Molecular Sciences* **13** (4), 4508–4522.

Abo Markeb, A., Alonso, A., Sánchez, A. & Font, X. 2017 Adsorption process of fluoride from drinking water with magnetic core-shell Ce-Ti@Fe_3O_4 and Ce-Ti oxide nanoparticles. *Science of the Total Environment* **598**, 949–958.

Adak, M. K., Chakraborty, S., Sen, S. & Dhak, D. 2017a Synthesis and optimization of low-cost and high efficient zirconium-aluminium modified iron oxide nano adsorbent for fluoride removal from drinking water. *Advanced Materials Proceedings* **2**, 716–724.

Adak, M. K., Sen, A., Mukherjee, A., Sen, S. & Dhak, D. 2017b Removal of fluoride from drinking water using highly efficient nanoadsorbent, Al(III)-Fe(III)-La(III) trimetallic oxide prepared by chemical route. *Journal of Alloys and Compounds* **719**, 460–469.

Ali, I. 2012 New generation adsorbents for water treatment. *Chemical Reviews* **112** (10), 5073–5091.

Amrhar, O., Nassali, H. & Elyoubi, M. S. 2015 Application of nonlinear regression analysis to select the optimum absorption isotherm for Methylene Blue adsorption onto Natural Illitic Clay. *Bulletin de la Société Royale des Sciences de Liège* **84**, 116–130.

Ayoob, S., Gupta, A. & Bhat, V. T. 2008 A conceptual overview on sustainable technologies for the defluoridation of drinking water. *Critical Reviews in Environmental Science and Technology* **38** (6), 401–470.

Azari, A., Kalantary, R. R., Ghanizadeh, G., Kakavandi, B., Farzadkia, M. & Ahmadi, E. 2015 Iron–silver oxide nanoadsorbent synthesized by co-precipitation \process for fluoride removal from aqueous solution and its adsorption mechanism. *RSC Advances* **5** (106), 87377–87391.

Azizullah, A., Khattak, M. N. K., Richter, P. & Donat Peter, H. 2011 Water pollution in Pakistan and its impact on public health – a review. *Environment International* **37**, 479–497.

Banks, D., Reimann, C., Røyset, O., Skarphagen, H. & Sæther, O. M. 1995 Natural concentrations of major and trace elements in some Norwegian bedrock groundwaters. *Applied Geochemistry* **10** (1), 1–16.

Barbier, O., Arreola-Mendoza, L. & Del Razo, L. M. 2010 Molecular mechanisms of fluoride toxicity. *Chemico-Biological Interactions* **188** (2), 319–333.

Bashir, M. T., Ali, S. B., Adris, A. & Haroon, R. 2013 Health effects associated with fluoridated water sources–a review of Central Asia. *Asian Journal of Water, Environment and Pollution* **10** (3), 29–37.

Bhatnagar, A., Kumar, E. & Sillanpää, M. 2011 Fluoride removal from water by adsorption – a review. *Chemical Engineering Journal* **171** (3), 811–840.

Bia, G., De Pauli, C. P. & Borgnino, L. 2012 The role of Fe(III) modified montmorillonite on fluoride mobility: adsorption experiments and competition with phosphate. *Journal of Environmental Management* **100**, 1–9.

Boparai, H. K., Joseph, M. & O'Carroll, D. M. 2011 Kinetics and thermodynamics of cadmium ion removal by adsorption onto nano zerovalent iron particles. *Journal of Hazardous Materials* **186** (1), 458–465.

Camargo, J. A. 2003 Fluoride toxicity to aquatic organisms: a review. *Chemosphere* **50** (3), 251–264.

Chang, C.-F., Lin, P.-H. & Höll, W. 2006 Aluminum-type superparamagnetic adsorbents: synthesis and application on fluoride removal. *Colloids and Surfaces A: Physicochemical and Engineering Aspects* **280** (1), 194–202.

Chen, L., Wu, H.-X., Wang, T.-J., Jin, Y., Zhang, Y. & Dou, X.-M. 2009 Granulation of Fe–Al–Ce nanoadsorbent for fluoride removal from drinking water by spray coating on sand in a fluidized bed. *Powder Technology* **193** (1), 59–64.

Chen, L., He, B.-Y., He, S., Wang, T.-J., Su, C.-L. & Jin, Y. 2012 Fe–Ti oxide nanoadsorbent synthesized by co-precipitation for fluoride removal from drinking water and its adsorption mechanism. *Powder Technology* **227**, 3–8.

Chen, P., Wang, T., Xiao, Y., Tian, E., Wang, W., Zhao, Y., Tian, L., Jiang, H. & Luo, X. 2018 Efficient fluoride removal from aqueous solution by synthetic FeMgLa tri-metal nanocomposite and the analysis of its adsorption mechanism. *Journal of Alloys and Compounds* **738**, 118–129.

Ciopec, M., Negrea, A., Lupa, L., Davidescu, C. M. & Negrea, P. 2014 Studies regarding As (V) adsorption from underground water by Fe-XAD8-DEHPA impregnated resin. Equilibrium sorption and fixed-bed column tests. *Molecules* **19** (10), 16082–16101.

Devi, R. R., Umlong, I. M., Raul, P. K., Das, B., Banerjee, S. & Singh, L. 2014 Defluoridation of water using nano-magnesium oxide. *Journal of Experimental Nanoscience* **9** (5), 512–524.

Diesendorf, M., Colquhoun, J. & Spittle, B. 1998 Fluoridation and bones: authors' response to critics. *Aust NZJ Public Health* **22**, 165–167.

Edmunds, W. M. & Smedley, P. 2013 Fluoride in natural waters. In: *Essentials of Medical Geology* (O. Selinus, ed.). Springer, Netherlands, pp. 311–336.

El-Sikaily, A., El Nemr, A., Khaled, A. & Abdelwehab, O. 2007 Removal of toxic chromium from wastewater using green alga Ulva lactuca and its activated carbon. *Journal of Hazardous Materials* **148** (1), 216–228.

Emamjomeh, M. M. & Sivakumar, M. 2009 Fluoride removal by a continuous flow electrocoagulation reactor. *Journal of Environmental Management* **90** (2), 1204–1212.

EPA 2009 *National Primary Drinking Water Regulations*. Available from: http://water.epa.gov/drink/contaminants/.

Fawell, J., Bailey, K., Chilton, J., Dahi, E., Fewtrell, L. & Magara, Y. 2006 *Fluoride in Drinking-Water*. IWA Publishing, Colchester, UK.

Foo, K. Y. & Hameed, B. H. 2010 Insights into the modeling of adsorption isotherm systems. *Chemical Engineering Journal* **156** (1), 2–10.

Ghadam, A. & Idrees, M. 2013 Characterization of $CaCO_3$ nanoparticles synthesized by reverse microemulsion technique in different concentrations of surfactants. *Iranian Journal of Chemistry and Chemical Engineering* **32** (3), 27–35.

Gogoi, S., Nath, S. K., Bordoloi, S. & Dutta, R. K. 2015 Fluoride removal from groundwater by limestone treatment in presence of phosphoric acid. *Journal of Environmental Management* **152**, 132–139.

Goswami, A. & Purkait, M. K. 2012 The defluoridation of water by acidic alumina. *Chemical Engineering Research and Design* **90** (12), 2316–2324.

Gusmão, K. A. G., Gurgel, L. V. A., Melo, T. M. S. & Gil, L. F. 2013 Adsorption studies of methylene blue and gentian violet on sugarcane bagasse modified with EDTA dianhydride (EDTAD) in aqueous solutions: kinetic and equilibrium aspects. *Journal of Environmental Management* **118**, 135–143.

Hafshejani, L. D., Tangsir, S., Daneshvar, E., Maljanen, M., Lähde, A., Jokiniemi, J., Naushad, M. & Bhatnagar, A. 2017 Optimization of fluoride removal from aqueous solution by Al_2O_3 nanoparticles. *Journal of Molecular Liquids* **238**, 254–262.

Holt, P. K., Barton, G. W. & Mitchell, C. A. 2005 The future for electrocoagulation as a localised water treatment technology. *Chemosphere* **59** (3), 355–367.

Jagtap, S., Yenkie, M. K., Labhsetwar, N. & Rayalu, S. 2012 Fluoride in drinking water and defluoridation of water. *Chemical Reviews* **112** (4), 2454–2466.

Jain, M., Garg, V. K. & Kadirvelu, K. 2010 Adsorption of hexavalent chromium from aqueous medium onto carbonaceous adsorbents prepared from waste biomass. *Journal of Environmental Management* **91** (4), 949–957.

Keränen, A., Leiviskä, T., Hormi, O. & Tanskanen, J. 2015 Removal of nitrate by modified pine sawdust: effects of temperature and co-existing anions. *Journal of Environmental Management* **147**, 46–54.

Khalid, A., Kazmi, M. A., Habib, M. & Shahzad, K. 2015 Kinetic & equilibrium modelling of copper iosorption. *Journal of Faculty of Engineering & Technology* **22** (1), 131–145.

Kirboga, S. & Oner, M. 2013 Effect of the experimental parameters on calcium carbonate precipitation. *Chemical Engineering Transactions* **32**, 2119–2124.

Kontoyannis, C. G. & Vagenas, N. V. 2000 Calcium carbonate phase analysis using XRD and FT-Raman spectroscopy. *Analyst* **125** (2), 251–255.

Kumar, D. & Tomar, V. 2014 Removal of fluoride from potable water using smart nanomaterial as adsorbent. In: *Application of Nanotechnology in Water Research* (A. K. Mishra, ed.). John Wiley & Sons, Hoboken, NJ, pp. 285–308.

Kut, K. M. K., Sarswat, A., Srivastava, A., Pittman Jr., C. U. & Mohan, D. 2016 A review of fluoride in african groundwater and local remediation methods. *Groundwater for Sustainable Development* **2–3**, 190–212.

Li, Y.-H., Wang, S., Cao, A., Zhao, D., Zhang, X., Xu, C., Luan, Z., Ruan, D., Liang, J., Wu, D. & Wei, B. 2001 Adsorption of fluoride from water by amorphous alumina supported on carbon nanotubes. *Chemical Physics Letters* **350** (5–6), 412–416.

Li, Y., Zhang, P., Du, Q., Peng, X., Liu, T., Wang, Z., Xia, Y., Zhang, W., Wang, K. & Zhu, H. 2011 Adsorption of fluoride from aqueous solution by graphene. *Journal of Colloid and Interface Science* **363** (1), 348–354.

Maheshwari, R. 2006 Fluoride in drinking water and its removal. *Journal of Hazardous Materials* **137** (1), 456–463.

Mansoori, G. A., Bastami, T. R. & Ahmadpour, A. 2008 *Environmental Application of Nanotechnology*.

Meenakshi, S. & Viswanathan, N. 2007 Identification of selective ion-exchange resin for fluoride sorption. *Journal of Colloid and Interface Science* **308** (2), 438–450.

Mohapatra, M., Anand, S., Mishra, B., Giles, D. E. & Singh, P. 2009 Review of fluoride removal from drinking water. *Journal of Environmental Management* **91** (1), 67–77.

Oladoja, N., Chen, S., Drewes, J. & Helmreich, B. 2015 Characterization of granular matrix supported nano magnesium oxide as an adsorbent for defluoridation of groundwater. *Chemical Engineering Journal* **281**, 632–643.

Oruc, N. 2008 Occurrence and problems of high fluoride waters in Turkey: an overview. *Environmental Geochemistry and Health* **30** (4), 315–323.

Pontie, M., Dach, H., Lhassani, A. & Diawara, C. K. 2013 Water defluoridation using nanofiltration vs. reverse osmosis: the first world unit, Thiadiaye (Senegal). *Desalination and Water Treatment* **51** (1–3), 164–168.

Rafique, A., Awan, M. A., Wasti, A., Qazi, I. A. & Arshad, M. 2012 Removal of fluoride from drinking water using modified immobilized activated alumina. *Journal of Chemistry* **2013** article 386476. https://doi.org/10.1155/2013/386476.

Rao, T., Kasiviswanath, I. & Murthy, Y. 2009 *Defluoridation of Water by Nanotechnology*.

Reardon, E. J. & Wang, Y. 2000 A limestone reactor for fluoride removal from wastewaters. *Environmental Science & Technology* **34** (15), 3247–3253.

Reyes Bahena, J. L., Robledo Cabrera, A., López Valdivieso, A. & Herrera Urbina, R. 2002 Fluoride adsorption onto α-Al2O3 and its effect on the zeta potential at the alumina–aqueous electrolyte interface. *Separation Science and Technology* **37** (8), 1973–1987.

Sani, T., Gómez-Hortigüela, L., Mayoral, Á., Chebude, Y., Pérez-Pariente, J. & Díaz, I. 2017 Controlled growth of nano-hydroxyapatite on stilbite: defluoridation performance. *Microporous and Mesoporous Materials* **254**, 86–95.

Saucier, C., Adebayo, M. A., Lima, E. C., Cataluña, R., Thue, P. S., Prola, L. D. T., Puchana-Rosero, M. J., Machado, F. M., Pavan, F. A. & Dotto, G. L. 2015 Microwave-assisted activated carbon from cocoa shell as adsorbent for removal of sodium diclofenac and nimesulide from aqueous effluents. *Journal of Hazardous Materials* **289**, 18–27.

Sundaram, C. S., Viswanathan, N. & Meenakshi, S. 2008 Defluoridation chemistry of synthetic hydroxyapatite at nano scale: equilibrium and kinetic studies. *Journal of Hazardous Materials* **155** (1), 206–215.

Sundaram, C. S., Viswanathan, N. & Meenakshi, S. 2009 Fluoride sorption by nano-hydroxyapatite/chitin composite. *Journal of Hazardous Materials* **172** (1), 147–151.

Taglieri, G., Mondelli, C., Daniele, V., Pusceddu, E. & Trapananti, A. 2013 Synthesis and X-ray diffraction analyses of calcium hydroxide nanoparticles in aqueous suspension. *Advances in Materials Physics and Chemistry* **3**, 108–112.

Tangsir, S., Hafshejani, L. D., Lähde, A., Maljanen, M., Hooshmand, A., Naseri, A. A., Moazed, H., Jokiniemi, J. & Bhatnagar, A. 2016 Water defluoridation using Al2O3 nanoparticles synthesized by flame spray pyrolysis (FSP) method. *Chemical Engineering Journal* **288**, 198–206.

Tembhurkar, A. & Dongre, S. 2006 Studies on fluoride removal using adsorption process. *Journal of Environmental Science & Engineering* **48** (3), 151–156.

Tiemann, M. 2011 *Fluoride in Drinking Water: A Review of Fluoridation and Regulation Issues*. Service CR, Washington, DC.

Tiemann, M. 2013 *Fluoride in Drinking Water: A Review of Fluoridation and Regulation Issues*. BiblioGov, Washington, DC.

Ullah, R., Malik, R. N. & Qadir, A. 2009 Assessment of groundwater contamination in an industrial city, Sialkot, Pakistan. *African Journal of Environmental Science and Technology* **3** (12), 429–446.

Uvarov, V. & Popov, I. 2007 Metrological characterization of X-ray diffraction methods for determination of crystallite size in nano-scale materials. *Materials Characterization* **58** (10), 883–891.

Wang, A., Xia, T., Chu, Q., Zhang, M., Liu, F., Chen, X. & Yang, K. 2004 Effects of flueoride on lipid peroxidation, DNA damige and apoptosis in human embryo hepatocytes. *Biomedical and Environmental Sciences* **17** (2), 217–222.

Wu, F.-C., Liu, B.-L., Wu, K.-T. & Tseng, R.-L. 2010 A new linear form analysis of Redlich–Peterson isotherm equation for the adsorptions of dyes. *Chemical Engineering Journal* **162** (1), 21–27.

Yan, L., Tu, H., Chan, T. & Jing, C. 2017 Mechanistic study of simultaneous arsenic and fluoride removal using granular TiO_2-La adsorbent. *Chemical Engineering Journal* **313**, 983–992.

Zhang, C., Chen, L., Wang, T.-J., Su, C.-L. & Jin, Y. 2014 Synthesis and properties of a magnetic core–shell composite nanoadsorbent for fluoride removal from drinking water. *Applied Surface Science* **317**, 552–559.

Zhang, C., Li, Y., Wang, T.-J., Jiang, Y. & Fok, J. 2017 Synthesis and properties of a high-capacity iron oxide adsorbent for fluoride removal from drinking water. *Applied Surface Science* **425**, 272–281.

Zuo, Q., Chen, X., Li, W. & Chen, G. 2008 Combined electrocoagulation and electroflotation for removal of fluoride from drinking water. *Journal of Hazardous Materials* **159** (2), 452–457.

First received 28 May 2019; accepted in revised form 7 December 2019. Available online 27 December 2019